crystals

MDPI

Article

The Influence of $BaTiO_3$ Content on the Energy Storage Properties of $Bi_{0.5}Na_{0.5}TiO_3$-$Bi(Mg_{2/3}Nb_{1/3})O_3$ Lead-Free Ceramics

Zhuo Li [1,2,*], Dandan Zhang [1], Chenbo Wang [1], Jiayong Zhang [1], Zixuan Wang [1], Zhuo Wang [1,2], Xin Yan [1,2], Tao Ai [1,2], Dawei Wang [3], Zhilun Lu [4,*] and Yanhui Niu [1,2]

1 School of Materials Science and Engineering, Chang'an University, Xi'an 710061, China
2 Engineering Research Center of Transportation Materials of Ministry of Education, Chang'an University, Xi'an 710061, China
3 Functional Materials and Acousto-Optic Instruments Institute, School of Instrumentation Science and Engineering, Harbin Institute of Technology, Harbin 150080, China
4 School of Computing, Engineering and the Built Environment, Edinburgh Napier University, Edinburgh EH10 5DT, UK
* Correspondence: lizhuo@chd.edu.cn (Z.L.); z.lu@napier.ac.uk (Z.L.)

Abstract: $Na_{0.5}Bi_{0.5}TiO_3$ (NBT)-based ceramics are promising lead-free candidates for energy-storage applications due to their outstanding dielectric and ferroelectric properties derived from large polarization. However, the high coercive field and large remnant polarization are unfavorable for practical applications, and thus NBT-based ceramics with relaxation behavior via doping/forming solid solutions with other elements/components have been widely studied. In this work, $BaTiO_3$ (BT) was introduced to the $0.94Na_{0.5}Bi_{0.5}TiO_3$-$0.06Bi(Mg_{2/3}Nb_{1/3})O_3$ system by a conventional solid-state reaction to form a homogeneous solid solution of $0.94[(1-x)Na_{0.5}Bi_{0.51}TiO_3$-$xBaTiO_3]$-$0.06Bi(Mg_{2/3}Nb_{1/3})O_3$ (BNT-100xBT-BMN). As the BT content increased, the proportion of the rhombohedral *R3c* phase increased while that of the tetragonal *P4bm* phase decreased, leading to the maximum P_{max} (38.29 μC/cm^2) and E_b (80 kV/cm) obtained in BNT-7BT-BMN (x = 0.07) composition. Specifically, the optimal energy storage properties of W_{rec} ~ 1.02 J/cm^3 and η ~ 62.91% under 80 kV/cm were obtained in BNT-7BT-BMN ceramics, along with good temperature stability up to 200 °C, which are promising factors for future pulse power applications.

Keywords: energy storage; phase structure; dielectric properties; $Bi_{0.5}Na_{0.5}TiO_3$

Citation: Li, Z.; Zhang, D.; Wang, C.; Zhang, J.; Wang, Z.; Wang, Z.; Yan, X.; Ai, T.; Wang, D.; Lu, Z.; et al. The Influence of $BaTiO_3$ Content on the Energy Storage Properties of $Bi_{0.5}Na_{0.5}TiO_3$-$Bi(Mg_{2/3}Nb_{1/3})O_3$ Lead-Free Ceramics. *Crystals* **2023**, *13*, 733. https://doi.org/10.3390/cryst13050733

Academic Editor: Maria Gazda

Received: 28 March 2023
Revised: 15 April 2023
Accepted: 22 April 2023
Published: 27 April 2023

1. Introduction

Energy storage materials have attracted widespread attention because of the increasing demand for energy. Among the various electrical energy storage materials, dielectric ceramic capacitors play an important role in advanced electronic and electrical devices owing to their small volume, ultrahigh power densities, and fast charge–discharge ability [1–7], and thus they have been widely used in the fields of hybrid electric vehicles, laser weapons, mobile electronics, and pulse power technology [8–10]. Thereinto, lead-based ferroelectric ceramics have been intensively investigated due to their excellent energy storage performance at room temperature [11,12]. Unfortunately, lead-based ferroelectric ceramics containing lead elements are harmful to both humans and the environment, and many countries have banned their use [13,14]. Therefore, it is urgent that researchers seek some material that can replace lead-based ceramics. Sodium bismuth titanate ($Bi_{0.5}Na_{0.5}TiO_3$, BNT) with a typical ABO_3-type perovskite structure has been regarded as a good alternative to lead-based ceramics because of its prominent dielectric and ferroelectric performance [15], such as large polarization derived from the orbital hybridization between a $6s^2$ long pair of A-site Bi^{3+} and the 2p electron of O^{2-} [16,17], which is beneficial to energy storage

performance. However, the high coercive field (E_c) renders its application in electronic equipment impractical [18].

As an energy storage material, large saturated polarization, low remnant polarization (P_r) and high electric breakdown field strength (E_b) are required according to the related equations [10,19,20], by which the energy storage density (W_{rec}) and efficiency (η) of the dielectric capacitor can be obtained. Evidently, in order to enhance the energy storage properties, the key issue to be solved is to reduce P_r and E_c, which guides researchers to design BNT-based energy storage materials with the characteristic of slim polarization hysteresis loops. Correspondingly, a series of BNT-based solid solutions have been designed by forming relaxor ferroelectrics (RFE) [21–30]. Chandrasekhar et al. reported the energy storage performance of BNT-$BaTiO_3$ (BNT-BT) binary system ceramics [21]. Based on this, Xu et al. designed (1−x)BNT-BT-x$NaNbO_3$ relaxor ferroelectric ceramics, and the optimum energy storage properties were obtained in the ceramics with x = 0.10 [22]. Then, BNBT-0.06$KNbO_3$ ceramics were prepared and the energy storage performance with W_{rec} of 0.89 J/cm^3 at 100 kV/cm was observed [23]. In addition, Wang et al. [24] employed the conventional solid-state reaction method to fabricate BNT-BT-0.1$Na_{0.73}Bi_{0.09}NbO_3$ lead-free ceramics, and the optimal W_{rec} reached up to 1.56 J/cm^3 with an energy efficiency of η = 92.5% at 120 kV/cm. Moreover, $(Y_{0.5}Ta_{0.5})^{4+}$ complex ions were introduced into BNT-BT ceramics and an improved W_{rec} of 1.41 J/cm^3 at 98 kV/cm was obtained [25]. Obviously, these studies selected BNT-BT as the matrix and included additional elements/compositions to increase the energy storage properties, but they paid little attention to the influence of BT content on the energy storage properties. Furthermore, the introduction of $Bi(Mg_{2/3}Nb_{1/3})O_3$ in BNT ceramics would induce the phase transition and optimize the energy storage density of the system [26].

Based on the above analysis, in this work, $BaTiO_3$ was introduced to the $0.94Na_{0.5}Bi_{0.5}TiO_3$-$0.06Bi(Mg_{2/3}Nb_{1/3})O_3$ system and the composition of $0.94[(1-x)Na_{0.5}Bi_{0.51}TiO_3$-x$BaTiO_3]$-$0.06Bi(Mg_{2/3}Nb_{1/3})O_3$ was designed. In addition, the influence of $BaTiO_3$ content on phase structure, microstructure, dielectric, ferroelectric properties, and energy storage properties was investigated in detail.

2. Materials and Methods

$0.94[(1-x)Na_{0.5}Bi_{0.5}TiO_3$-x$BaTiO_3]$-$0.06Bi(Mg_{2/3}Nb_{1/3})O_3$ (abbreviated as BNT-100xBT-BMN, x = 0, 0.03, 0.05, 0.07) ceramics were fabricated via the conventional solid-state reaction [31]. The raw materials, including TiO_2 (>98.0%, Sinopharm Chemical Reagent Co., Ltd., Shanghai, China), Bi_2O_3 (>99.9%, Sinopharm Chemical Reagent Co., Ltd.), Na_2CO_3 (>99.8%, Sinopharm Chemical Reagent Co., Ltd.), $BaTiO_3$ (>99.5%, Sinopharm Chemical Reagent Co., Ltd.), MgO (>98.5%, Sinopharm Chemical Reagent Co., Ltd.), and Nb_2O_5 (>99.5%, Sinopharm Chemical Reagent Co., Ltd.) were weighed according to the stoichiometric ratio and then ball milled with ZrO_2 balls in alcohol (>99.7%, Tianjin Fuyu Fine Chemical Co., Ltd., Tianjin, China) at the speed of 300 r/min for 8 h. After being dried and sieved (120 mesh), the mixtures were sintered at 800 °C for 2 h. The sintered powders were ball milled for 8 h again, dried, sieved (200 mesh), and then sintered at 850 °C for 2 h. The obtained powers were ball milled in alcohol for 6 h and dried. Afterward, the powers were uniaxially pressed into 13mm-diameter pellets under a pressure of ~300 MPa with 6 wt% polyvinyl alcohol (PVA) as the binder. Finally, the pellets were sintered at 1080–1140 °C for 2 h after being heated at 550 °C for 3 h to burn out the PVA. To inhibit the volatilization of sodium and bismuth, the pellets were covered by the corresponding powers during sintering.

The phase structure of the sintered ceramic samples was identified by X-ray diffraction (XRD; D8 Advance, Bruker AXS, Karlsruhe, Germany) operated at 40 kV with CuKα radiation (λ = 1.5406 Å) and the scanning speed was 0.02°/s. The Rietveld refinement of XRD patterns was performed by the General Structure Analysis System (GSAS) software. The microstructure and elemental composition mapping of the free surface of sintered samples were observed by scanning electron microscopy (SME; S-4800, Hitachi, Japan) operated at

10 kV in the secondary electron mode, equipped with energy-dispersive X-ray spectroscopy (EDS; FeatureMax, Oxfordshire, UK). The average grain size distributions were determined by using analytical software (Nano Measurer). Before electrical measurements, the obtained ceramic samples were polished to 0.5 mm in thickness and coated with silver paste on both sides and then fired at 850 °C for 10 min. The dielectric temperature-dependent and frequency-dependent spectra were measured in the air atmosphere by a precise LCR meter (E4294, Agilent, Santa Clara, USA) from 25 °C to 500 °C. The polarization hysteresis loops were detected using a ferroelectric analyzer (TF-3000, AixACCT, Aachen, Germany) at 1 Hz from 20 °C to 200 °C.

3. Results

Figure 1a shows XRD patterns measured at room temperature of BNT-100xBT-BMN (x = 0, 0.03, 0.05, and 0.07) ceramics with the maximum bulk density. As can be seen from the patterns, all the samples exhibit a perovskite structure, suggesting that BT has successfully diffused into the BNT-BMN ceramic lattices. Additionally, all the diffraction peaks shift towards lower angles with the increase in BT content, indicating that the lattice parameters increased due to the fact that A-site complex ions (the radius: Bi^{3+} = 1.36 Å, Na^{+} = 1.39 Å) are replaced by the larger Ba^{2+} (the radius: 1.61 Å) [32–34]. In addition, it is clear that the (111) diffraction peak around 39.5°– 40.5° gradually splits into (003) and (021) peaks with the addition of BT, as displayed in the magnified views in Figure 1b. Meanwhile, the (200) peak at around 46°–47° for all the ceramics splits into (002) and (200) peaks, as shown in Figure 1c. All these typical features implied that BNT-100xBT-BMN (x = 0, 0.03, 0.05, and 0.07) ceramics were the two-phase coexistence of a tetragonal structure and a rhombohedral structure [16,35]. In order to further understand the crystal structure of BNT-100xBT-BMN ceramics, the tetragonal *P4bm* and rhombohedral *R3c* were selected to conduct the Rietveld refinement of XRD data by the GSAS software. As shown in Figure 1d,e, the reliability factor of weighted patterns (R_{wp}), the reliability factor of patterns (R_p), and the goodness-of-fit indicator (χ^2) for x = 0.03 and x = 0.07 ceramics are 7.40% and 6.48%, 5.92% and 5.18%, and 1.682 and 1.553, respectively, suggesting the structural model is valid and the refinement result is reliable. The obtained lattice parameters a, b, and c for both *P4bm* and *R3c* are displayed in Table 1. This result is consistent with the phenomenon that the diffraction peak moves to a lower degree as the BT content increases in Figure 1.

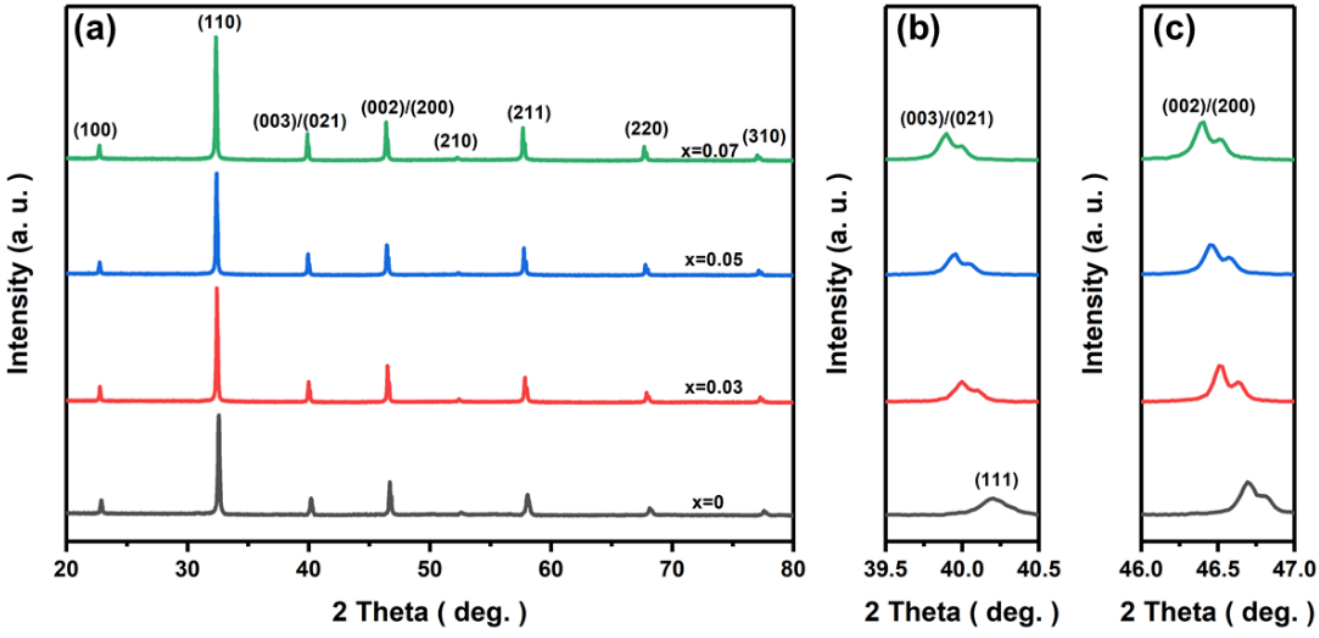

Figure 1. *Cont.*

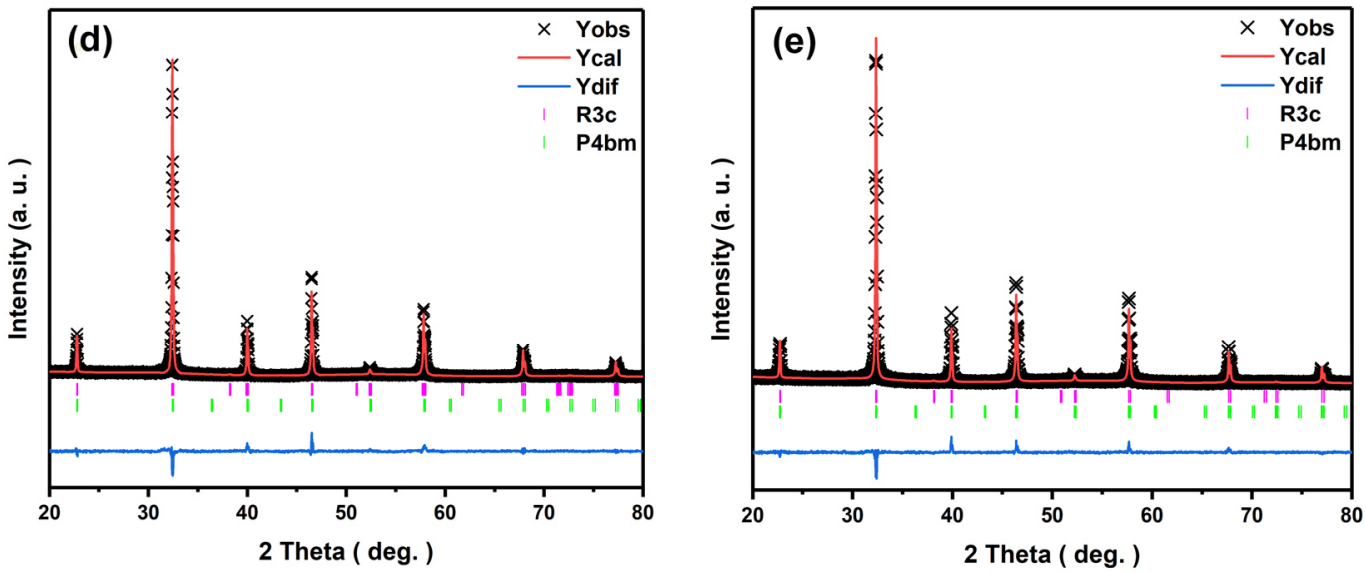

Figure 1. (**a**) XRD patterns of BNT-100xBT-BMN ceramic samples at room temperature; the enlarged region at 2θ range (**b**) from 39.5° to 40.5° and (**c**) from 46° to 47°; the Rietveld refinement results of (**d**) x = 0.03 and (**e**) x = 0.07 ceramics.

Table 1. Results of Rietveld refinement of XRD data for BNT-100xBT-BMN ceramics using R3c and P4bm space group.

Compositions	The Relative Content (%)	a = b (Å)	c (Å)	R_{wp}(%)	R_p(%)	χ^2
x = 0.03	R3c: 42.23% P4bm: 57.77%	5.516 5.519	13.551 3.903	7.40%	5.92%	1.682
x = 0.05	R3c: 46.51% P4bm: 53.49%	5.526 5.526	13.537 3.910	6.49%	5.51%	1.401
x = 0.07	R3c: 50.07% P4bm: 49.93%	5.533 5.554	13.554 3.915	6.48%	5.18%	1.553

The microstructure of the natural surface of the BNT-100xBT-BMN ceramic samples is shown in Figure 2. It can be found that all samples exhibit block-shaped grains and the grain size of BNT-100xBT-BMN ceramics gradually decreases with increasing BT content. As insets of Figure 2a–d display, the average grain size of BNT-100xBT-BMN ceramics is approximately 0.955 μm, 0.803 μm, 0.725μm, and 0.695 μm for x = 0, 0.03, 0.05, and 0.07, respectively. Because the system has a multicomponent and very complicated nature, the grain size refinement can be due to many reasons. A possible reason is that Ba^{2+} has a lower diffusion rate during the sintering process due to the higher ionic radius and atomic weight, which inhibits the growth of grains [36]. Commonly, small grain size and uniform grain distribution are beneficial to enhance the density of ceramics, thus improving the dielectric breakdown strength and energy storage density of ceramics [37–39]. Figure 2e displays the EDS mapping images of x = 0.07 ceramics. Clearly, all elements, including Bi, Na, Ti, Ba, Mg, Nb, and O, are distributed homogeneously. Moreover, the uniform distribution of the Ba element suggests that $BaTiO_3$ has been successfully diffused into the BNT-BMN lattices, which is consistent with the results of the XRD pattern.

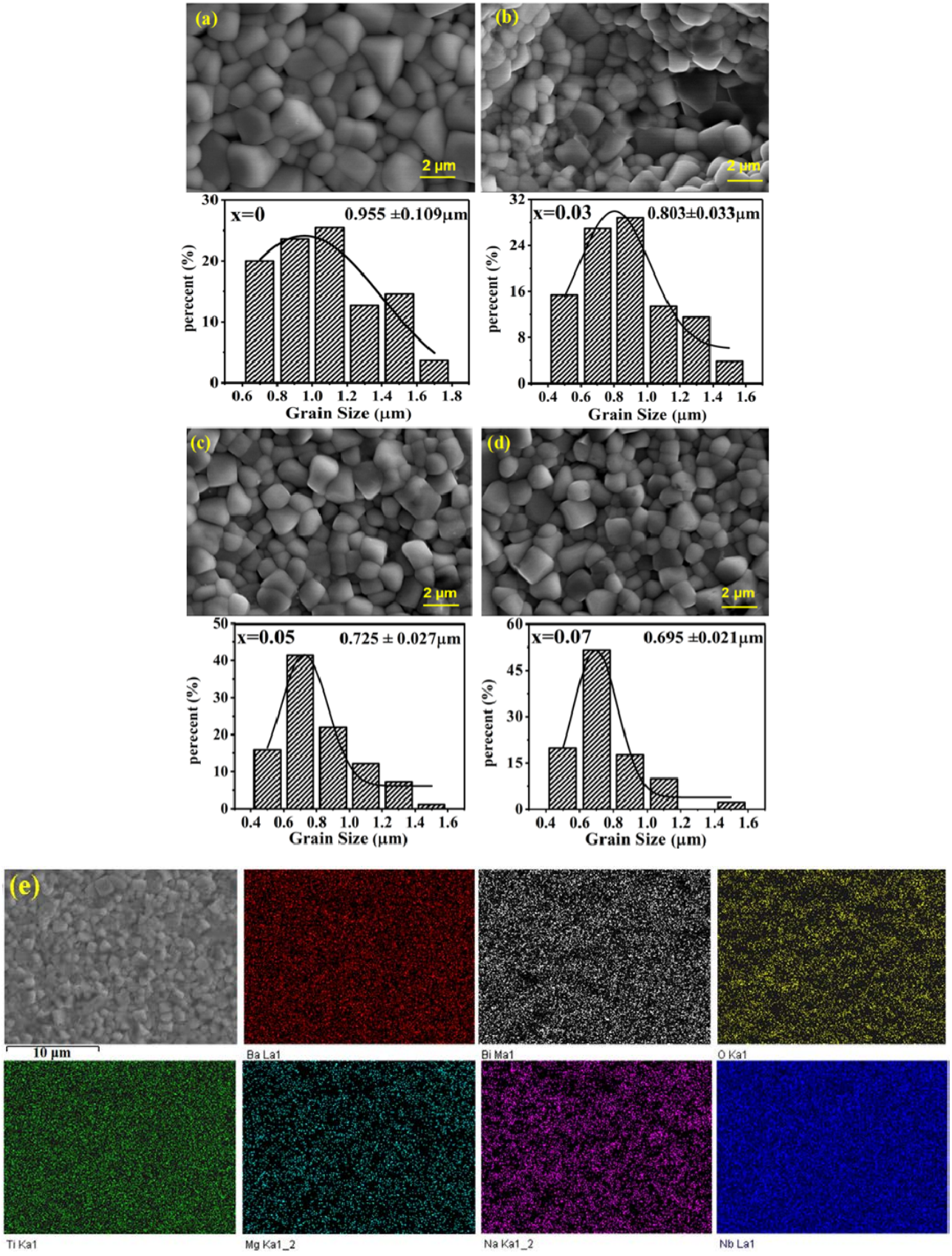

Figure 2. SEM micrographs of the free surface and grain size distribution for BNT-100xBT-BMN ceramics, (**a**) x = 0, (**b**) x = 0.03, (**c**) x = 0.05, (**d**) x = 0.07; (**e**) EDS mapping of the x = 0.07 ceramics.

Figure 3 shows the temperature-dependent dielectric properties of BNT-100xBT-BMN ceramics at different frequencies (1 KHz–100 kHz). For all the ceramic samples, there are two dielectric anomalies, which were derived from the thermal evolution and mutual transformation of two kinds of polar nanoregions with different symmetries [40]. The first dielectric anomaly peak is T_s, which is generally considered to be caused by the thermal evolution of the *P4bm* and *R3c* PNRs. The second dielectric anomaly peak appears at temperature T_m, and T_m is the temperature at which the permittivity reaches a maximum value. With the increase in BT content, T_s and T_m move towards low temperatures from 338 °C for x = 0 to 277 °C for x = 0.03 and 271 °C for x = 0.05 to 269 °C for x = 0.07 ceramics. Moreover, as frequency increases, the first dielectric anomaly peak T_s moves towards a high temperature, which is one of the distinctive features characterizing relaxor ferroelectrics. In addition, the dielectric constant of BNT-100xBT-BMN ceramics generally increased with the increase in BT, which is likely due to the fact that the Bi^{3+} and Na^{+} at the A-site in ABO_3 are replaced by Ba^{2+} with a larger radius, resulting in a larger local deformation of the unit cell [41]. The dielectric constants of x = 0, 0.03, 0.05, and 0.07 at room temperature under 1 kHz are 875, 1209, 1458, and 1554, respectively.

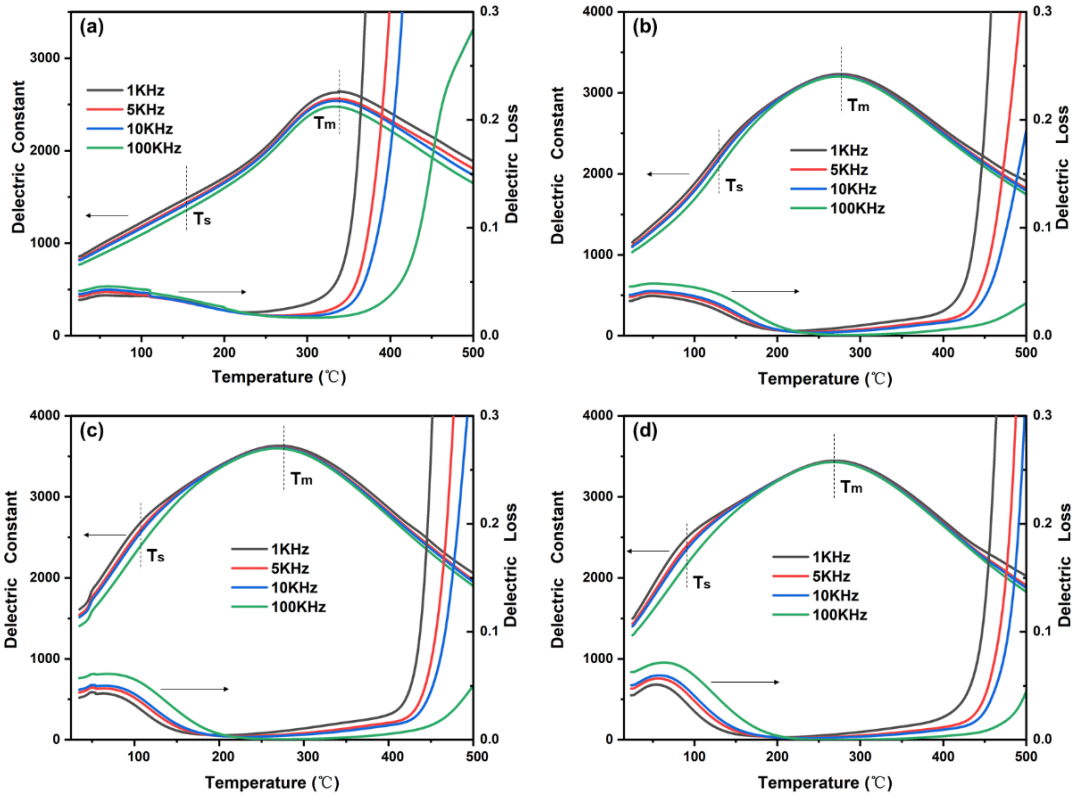

Figure 3. The dielectric constant and dielectric loss as a function of temperature under different frequencies for BNT-100xBT-BMN ceramics, (**a**) x = 0, (**b**) x = 0.03, (**c**) x = 0.05, (**d**) x = 0.07.

The polarization-electric field (P-E) hysteresis loops of BNT-100xBT-BMN ceramics measured under 40 kV/cm at room temperature are given in Figure 4a. Apparently, with the increase in BT content, the P_{max} increases prominently while the P_r increases inconspicuously, which could facilitate the improvement of energy storage density in BNT-100xBT-BMN ceramics (in Figure 4b) [16,42]. As is known, the improvement of W_{rec} requires not only high P_{max} and low P_r but also high E, which is also one of the key parameters in determining the performance of energy storage ceramics [35]. Hence, the P-E loops of the x = 0.07 ceramics under different electric fields are displayed in Figure 5. It can be found that with increasing electric fields, the P-E loops become slender, and P_{max} associated with ΔP increases significantly while P_r increases slightly. Ultimately, under an

electric field of 80 kV/cm, P_{max} and ΔP reach their maximums (Figure 5b) at 38.29 μC/cm^2 and 33.26 μC/cm^2, respectively. Correspondingly, the good energy storage performance at a low electric field of 80 kV/cm was obtained in x = 0.07 ceramics (W_{rec} = 1.022 J/cm^3, η = 62.90%), as shown in Figure 5c. It manifests that the x = 0.07 relaxor ceramics can be regarded as a promising candidate material for energy storage devices.

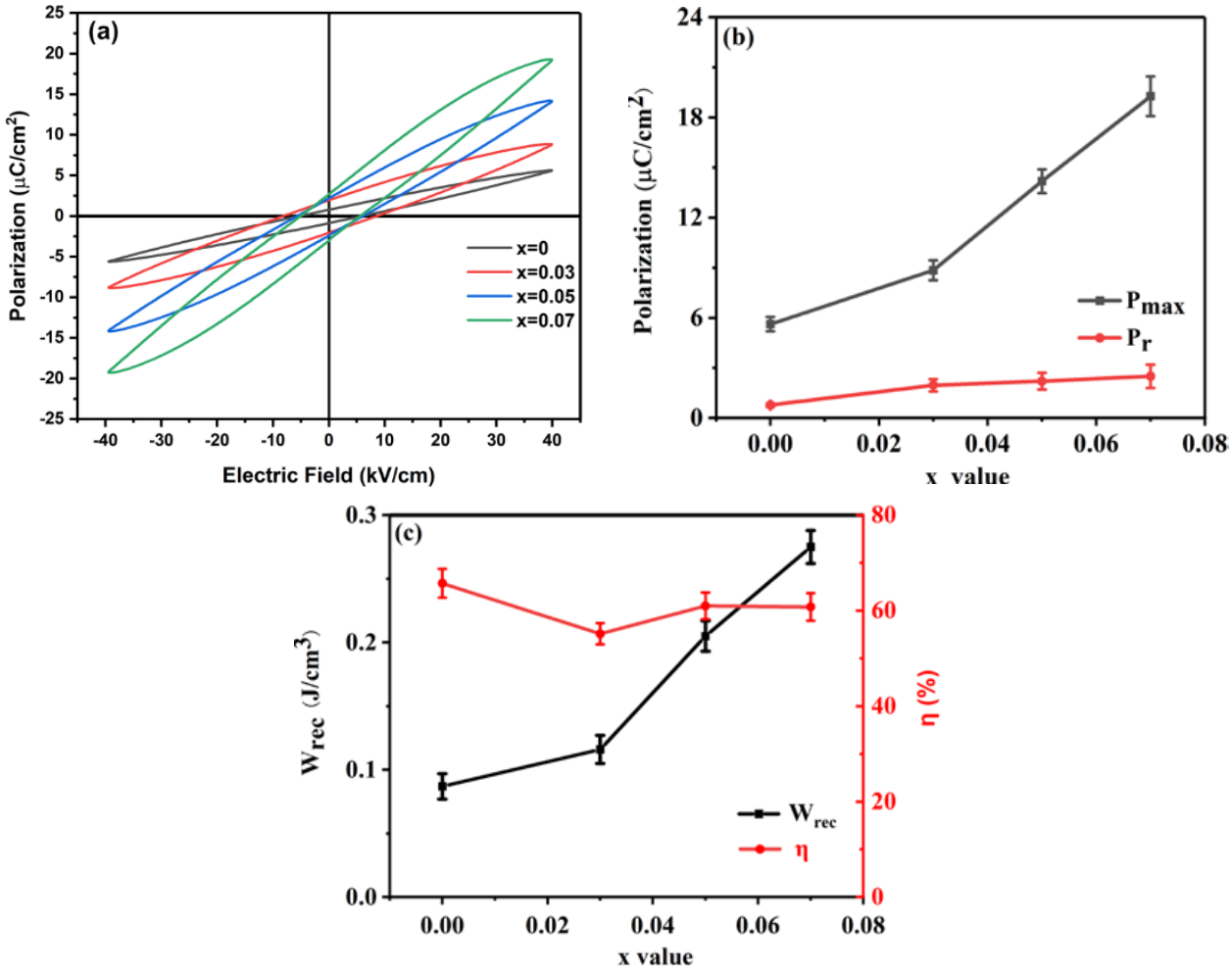

Figure 4. (**a**) P-E loops of BNT-100xBT-BMN ceramics at room temperature; (**b**) P_{max} and P_r of the BNT-100xBT-BMN ceramics; (**c**) W_{rec} and η of the BNT-100xBT-BMN ceramics.

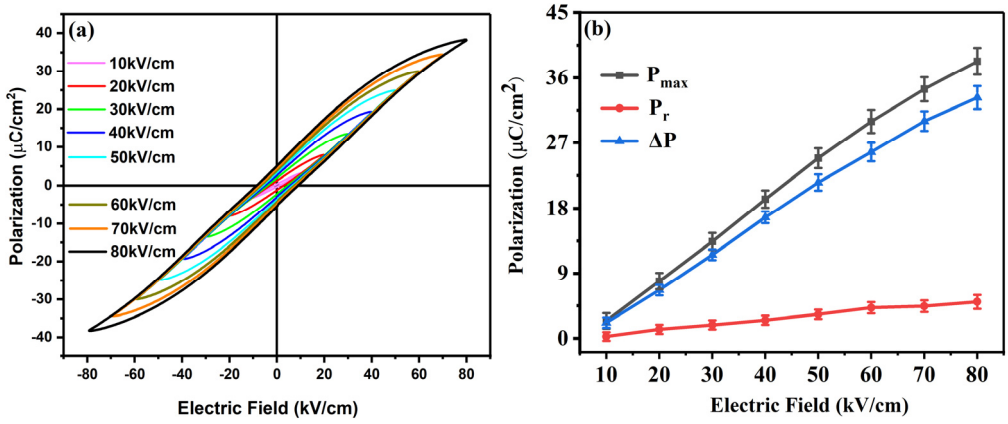

Figure 5. *Cont.*

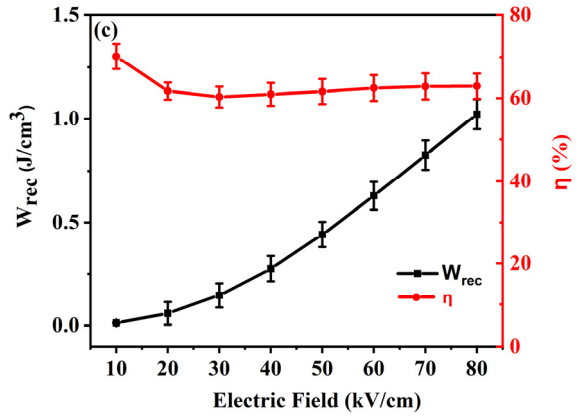

Figure 5. (**a**) P-E loops of x = 0.07 ceramics measured under different electric fields; (**b**) P_{max} and P_r under different electric fields; (**c**) the variation of W_{rec} and η under the electric fields.

In view of their practical application in electronic systems, especially pulsed power systems, thermal stability is also an important indicator of energy storage performance. Figure 6a depicts the temperature-dependent bipolar P-E loops for x = 0.07 ceramics under the applied E of 50 kV/cm in the temperature range of 25–200 °C. It can be found that the P-E loops become more constricted and slimmer as the temperature increases up to 125 °C, suggesting that the weakly polar phase increases during the heating process at a temperature lower than the T_d and thus suppresses the domain inversion under the external electric field [35,43–45]. However, above 125 °C, the constricted P-E loop gradually opened, and P_r increased (Figure 6b), which might be attributed to the movement of heat-activated carriers, leading to an increase in conduction and leakage loss, as can be seen in Figure 6d [44,45]. Interestingly, an identical variation in the temperature dependence of W_{rec} and η occurred (Figure 6c), that is both W_{rec} and η increase with increasing temperature up to 125 °C (W_{rec} = 0.55 J/cm^3 and η = 91.05% at 125 °C) and then decrease as the temperature further increased. Apparently, a thermal stability test exhibited a variation of more than 15% in W_{rec}, which may be due to the inappropriately working E. It has been reported that there is an appropriate E under which the W_{rec} of the ceramics can almost remain unchanged with increasing/decreasing temperature, and the opportune E is found to be slightly higher than the forward switching field and lower than the saturated electric field, such as in $Pb_{0.97}La_{0.02}(Zr_{0.58}Sn_{0.335}Ti_{0.085})O_3$ antiferroelectric ceramics [46]. Hence, the P-E loops of x = 0.07 ceramics at 125 °C under various electric fields (10 kV/cm~50 kV/cm) have been measured (shown in Figure 7a). Clearly, the P-E loops are all very slim, and as the electric field increases, the P_{max} increases sharply while the P_r has little change (Figure 7b) leading to the maximum W_{rec} obtained under the electric field of 50 kV/cm, which indicates that the applied E (50 kV/cm) is too low to maintain the temperature stability of the W_{rec}.

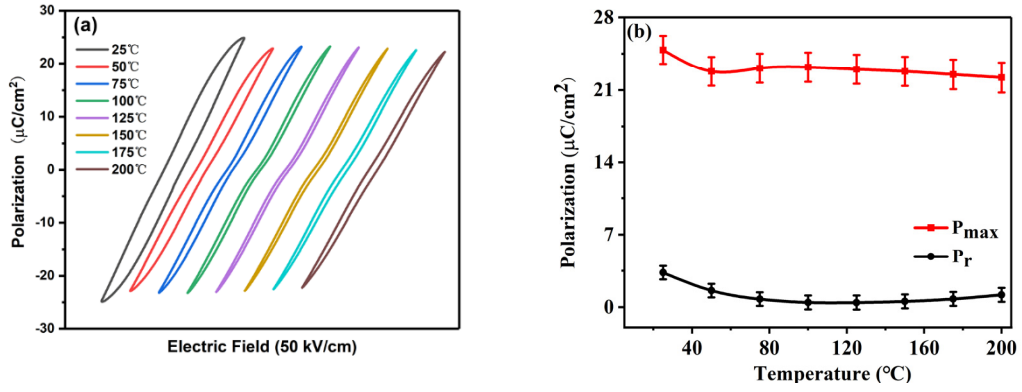

Figure 6. *Cont.*

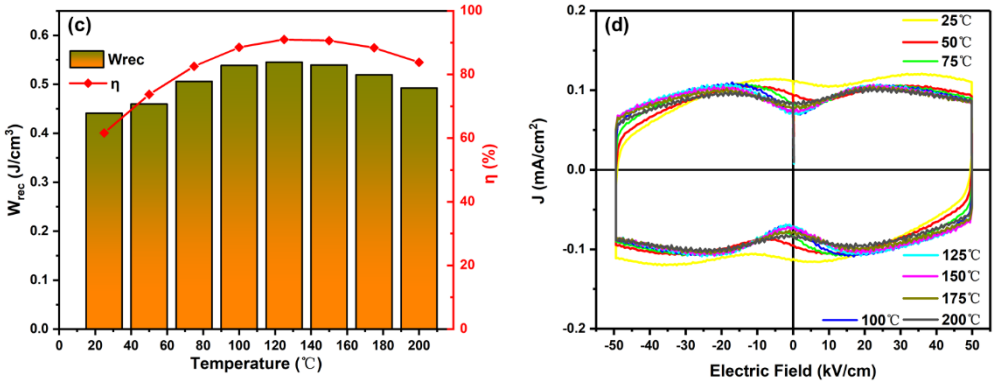

Figure 6. (**a**) P-E loops of x = 0.07 ceramics measured under different temperatures; (**b**) P_{max} and P_r at different temperatures; (**c**) W_{rec} and η of x = 0.07 ceramics under 50 kV/cm at temperature ranges of 25–200 °C; (**d**) J-E loops of x = 0.07 ceramics measured under different temperatures.

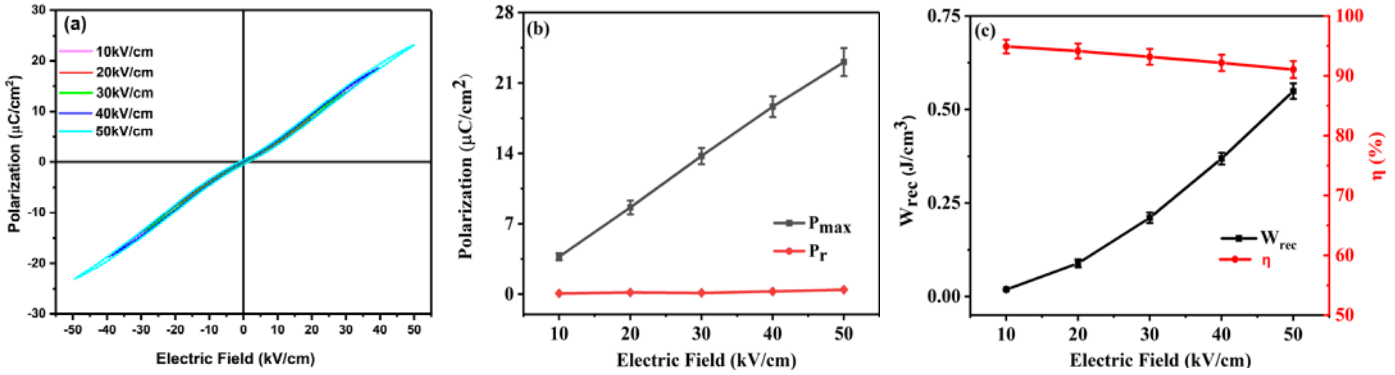

Figure 7. (**a**) P-E loops of x = 0.07 ceramics measured under different electric fields at 125 °C; (**b**) P_{max} and P_r under different electric fields; (**c**) W_{rec} and η of x = 0.07 ceramics under different electric fields at 125 °C.

4. Conclusions

In summary, new lead-free relaxor ferroelectric BNT-100xBT-BMN ceramics were successfully synthesized by conventional solid-state reactions. All compositions exhibited the two-phase coexistence of tetragonal structure and rhombohedral structure. As the BT content increased, the proportion of the rhombohedral *R3c* phase increased, while that of the tetragonal *P4bm* phase decreased, and the grain size of BNT-100xBT-BMN ceramics decreased from 0.955 μm to 0.695 μm, leading to the maximum P_{max} and E_b in x = 0.07 composition. The optimal W_{rec} of 1.02 J/cm^3 and η of 62.91% under 80 kV/cm at room temperature were obtained in x = 0.07 ceramics. Moreover, thermal stability in W_{rec} under 50 kV/cm exhibited a variation of more than 15%, manifesting that a higher or lower working E could result in a temperature-sensitive W_{rec}, and the working E should be optimized to meet the practical requirement of thermally stable energy storage capacitors.

Author Contributions: Conceptualization, Z.L. (Zhuo Li) and C.W.; methodology, Z.L. (Zhuo Li), D.Z. and C.W.; investigation, D.Z. and J.Z.; data curation, Z.W. (Zixuan Wang), J.Z. and Z.W. (Zhuo Wang); writing—original draft preparation, D.Z.; writing—review and editing, Z.L. (Zhuo Li), D.W. and Z.L (Zhilun Lu); visualization, D.Z. and C.W; project administration, X.Y., T.A. and Y.N. and All authors have read and agreed to the published version of the manuscript.

Funding: This research was funded by the National Natural Science Foundations of China (Grant Nos. 52278427 and 11604022), the Natural Science Foundation of Shaanxi province, China (No. 2021JM-172), the Fundamental Research Funds for the Central Universities, CHD (Nos. 300102311404 and 300102310301), the Key Research and Development Projects of Shaanxi Province (No. 2022GY-424),

and Undergraduate Training Programs for Innovation and Entrepreneurship of Chang'an University (Nos. S202210710249 and X202210710580).

Data Availability Statement: The data that support the finding of this study are available from the corresponding author upon reasonable request.

Conflicts of Interest: The authors declare no conflict of interest.

References

1. Qiao, X.; Wu, D.; Zhang, F.; Niu, M.; Chen, B.; Zhao, X.; Liang, P.; Wei, L.; Chao, X.; Yang, Z. Enhanced energy density and thermal stability in relaxor ferroelectric $Bi_{0.5}Na_{0.5}TiO_3$-$Sr_{0.7}Bi_{0.2}TiO_3$ ceramics. *J. Eur. Ceram. Soc.* **2019**, *39*, 4778–4784. [CrossRef]
2. Sun, N.; Li, Y.; Liu, X.; Hao, X. High energy-storage density under low electric field in lead-free relaxor ferroelectric film based on synergistic effect of multiple polar structures. *J. Power Sources* **2020**, *448*, 227457. [CrossRef]
3. Zhang, L.; Wang, Z.; Li, Y.; Chen, P.; Cai, J.; Yan, Y.; Zhou, Y.; Wang, D.; Liu, G. Enhanced energy storage performance in Sn doped $Sr_{0.6}(Na_{0.5}Bi_{0.5})_{0.4}TiO_3$ lead-free relaxor ferroelectric ceramics. *J. Eur. Ceram. Soc.* **2019**, *39*, 3057–3063. [CrossRef]
4. Qi, H.; Zuo, R. Linear-like lead-free relaxor antiferroelectric $(Bi_{0.5}Na_{0.5})TiO_3$–$NaNbO_3$ with giant energy-storage density/efficiency and super stability against temperature and frequency. *J. Mater. Chem. A* **2019**, *7*, 3971–3978. [CrossRef]
5. Han, D.; Zhang, B.; Zhao, D.; Zhao, J.; Liu, Y.; Zheng, S.; Fan, L.; Wang, C.; Wang, D.; Meng, F. Superior energy storage properties of $(1-x)Ba_{0.85}Ca_{0.15}Zr_{0.1}Ti_{0.9}O_3-xBi(Mg_{2/3}Ta_{1/3})O_3$ lead-free ceramics. *J. Alloy. Compd.* **2023**, *946*, 169300. [CrossRef]
6. Lu, Z.; Sun, D.; Wang, G.; Zhao, J.; Zhang, B.; Wang, D. Energy storage properties in Nd doped $AgNbTaO_3$ lead-free antiferroelectrics with Nb-site vacancies. *J. Adv. Dielectr.* **2022**, *12*, 2242006. [CrossRef]
7. Zhang, B.; Chen, X.; Pan, Z.; Liu, P.; Mao, M.; Song, K.; Mao, Z.; Sun, R.; Wang, D.; Zhang, S. Superior high-temperature energy density in molecular semiconductor/polymer all-organic composites. *Adv. Funct. Mater.* **2022**, *33*, 2210050. [CrossRef]
8. Hu, D.; Pan, Z.; He, Z.; Yang, F.; Zhang, X.; Li, P.; Liu, J. Significantly improved recoverable energy density and ultrafast discharge rate of $Na_{0.5}Bi_{0.5}TiO_3$-based ceramics. *Ceram. Int.* **2020**, *46*, 15364–15371. [CrossRef]
9. Li, Q.; Wang, J.; Ma, Y.; Ma, L.; Dong, G.; Fan, H. Enhanced energy-storage performance and dielectric characterization of $0.94Bi_{0.5}Na_{0.5}TiO_3$–$0.06BaTiO_3$ modified by $CaZrO_3$. *J. Alloy. Compd.* **2016**, *663*, 701–707. [CrossRef]
10. Jiang, Z.; Yang, Z.; Yuan, Y.; Tang, B.; Zhang, S. High energy storage properties and dielectric temperature stability of $(1-x)(0.8Bi_{0.5}Na_{0.5}TiO_3$-$0.2Ba_{0.3}Sr_{0.7}TiO_3)-xNaNbO_3$ lead-free ceramics. *J. Alloy. Compd.* **2021**, *851*, 156821. [CrossRef]
11. Yang, Y.; Wang, H.; Bi, L.; Zheng, Q.; Fan, G.; Jie, W.; Lin, D. High energy storage density and discharging efficiency in La^{3+}/Nb^{5+}-co-substituted $(Bi_{0.5}Na_{0.5})0.94Ba_{0.06}TiO_3$ ceramics. *J. Eur. Ceram. Soc.* **2019**, *39*, 3051–3056. [CrossRef]
12. Li, Q.; Yao, Z.; Ning, L.; Gao, S.; Hu, B.; Dong, G.; Fan, H. Enhanced energy-storage properties of $(1-x)(0.7Bi_{0.5}Na_{0.5}TiO_3$-$0.3Bi_{0.2}Sr_{0.7}TiO_3)$-$xNaNbO_3$ lead-free ceramics. *Ceram. Int.* **2018**, *44*, 2782–2788. [CrossRef]
13. Chen, P.; Li, P.; Zhai, J.; Shen, B.; Li, F.; Wu, S. Enhanced dielectric and energy-storage properties in $BiFeO_3$-modified $Bi_{0.5}(Na_{0.8}K_{0.2})_{0.5}TiO_3$ thin films. *Ceram. Int.* **2017**, *43*, 13371–13376. [CrossRef]
14. Bai, W.; Wang, L.; Zhao, X.; Zheng, P.; Wen, F.; Li, L.; Zhai, J.; Ji, Z. Tailoring frequency-insensitive large field-induced strain and energy storage properties in $(Ba_{0.85}Ca_{0.15})(Zr_{0.1}Ti_{0.9})O_3$-modified $(Bi_{0.5}Na_{0.5})TiO_3$ lead-free ceramics. *Dalton Trans.* **2019**, *48*, 10160–10173. [CrossRef]
15. Dong, G.; Fan, H.; Liu, H.; Jia, Y. Enhanced temperature stable dielectric property and energy-storage performance of $(1-x)(0.66Bi_{0.5}Na_{0.5}TiO_3$–$0.34Sr_{0.7}Bi_{0.2}TiO_3)-xK_{0.5}Nd_{0.5}TiO_3$ lead-free relaxor electroceramics. *Ceram. Int.* **2020**, *46*, 23194–23199. [CrossRef]
16. Fan, X.; Li, P.; Du, J.; Chen, C.; Fu, P.; Hao, J.; Yue, Z.; Li, W. High-energy storage performance of $(1-x)[0.935(Bi_{0.5}Na_{0.5})TiO_3$–$0.065BaTiO_3]$–$xBa(Zr_{0.3}Ti_{0.7})O_3$ ceramics with wide temperature range. *J. Mater. Sci. Mater. Electron.* **2020**, *31*, 9974–9981. [CrossRef]
17. Zhou, X.; Qi, H.; Yan, Z.; Xue, G.; Luo, H.; Zhang, D. Large energy density with excellent stability in fine-grained $(Bi_{0.5}Na_{0.5})TiO_3$-based lead-free ceramics. *J. Eur. Ceram. Soc.* **2019**, *39*, 4053–4059. [CrossRef]
18. Zhao, Y.; Xu, J.; Zhou, C.; Yuan, C.; Li, Q.; Chen, G.; Wang, H.; Yang, L. High energy storage properties and dielectric behavior of $(Bi_{0.5}Na_{0.5})0.94Ba_{0.06}Ti_{1-x}(Al_{0.5}Nb_{0.5})_xO_3$ lead-free ferroelectric ceramics. *Ceram. Int.* **2016**, *42*, 2221–2226. [CrossRef]
19. Yan, F.; Huang, K.; Jiang, T.; Zhou, X.; Shi, Y.; Ge, G.; Shen, B.; Zhai, J. Significantly enhanced energy storage density and efficiency of BNT-based perovskite ceramics via A-site defect engineering. *Energy Storage Mater.* **2020**, *30*, 392–400. [CrossRef]
20. Huang, Y.; Li, F.; Hao, H.; Xia, F.; Liu, H.; Zhang, S. $(Bi_{0.51}Na_{0.47})TiO_3$ based lead free ceramics with high energy density and efficiency. *J. Materiomics* **2019**, *5*, 385–393. [CrossRef]
21. Chandrasekhar, M.; Kumar, P. Synthesis and characterizations of BNT–BT and BNT–BT–KNN ceramics for actuator and energy storage applications. *Ceram. Int.* **2015**, *41*, 5574–5580. [CrossRef]
22. Xu, Q.; Li, T.; Hao, H.; Zhang, S.; Wang, Z.; Cao, M.; Yao, Z.; Liu, H. Enhanced energy storage properties of NaNbO3 modified $Bi_{0.5}Na_{0.5}TiO_3$ based ceramics. *J. Eur. Ceram. Soc.* **2015**, *35*, 545–553. [CrossRef]
23. Wang, B.; Luo, L.; Jiang, X.; Li, W.; Chen, H. Energy-storage properties of $(1-x)Bi_{0.47}Na_{0.47}Ba_{0.06}TiO_3$–$xKNbO_3$ lead-free ceramics. *J. Alloy. Compd.* **2014**, *585*, 14–18. [CrossRef]
24. Wang, J.; Fan, H.; Hu, B.; Jiang, H. Enhanced energy-storage performance and temperature-stable dielectric properties of $(1-x)(0.94Na_{0.5}Bi_{0.5}TiO_3$–$0.06BaTiO_3)$–$xNa_{0.73}Bi_{0.09}NbO_3$ ceramics. *J. Mater. Sci. Mater. Electron.* **2018**, *30*, 2479–2488. [CrossRef]

25. Yan, B.; Fan, H.; Wang, C.; Zhang, M.; Yadav, A.; Zheng, X.; Wang, H.; Du, Z. Giant electro-strain and enhanced energy storage performance of $(Y_{0.5}Ta_{0.5})^{4+}$ co-doped $0.94(Bi_{0.5}Na_{0.5})TiO_3$-$0.06BaTiO_3$ lead-free ceramics. *Ceram. Int.* **2020**, *46*, 281–288. [CrossRef]
26. Li, Z.; Wang, Z.; Yang, Q.; Zhang, D.; Fang, M.; Li, Z.; Gao, B.; Zhang, J.; Lei, N.; Zheng, L.; et al. Phase transition and energy storage properties of $Bi_{0.5}Na_{0.5}TiO_3$–$Bi(Mg_{2/3}Nb_{1/3})O_3$ lead-free ceramics. *Ceram. Int.* **2023**, *49*, 9615–9621. [CrossRef]
27. Li, Z.; Yang, Q.; Wang, C.; Zhang, J.; Wang, Z.; Gao, B.; Li, Z.; Wang, Z.; Yan, X.; Ai, T.; et al. A Brief Review of Sodium Bismuth Titanate-Based Lead-Free Materials for Energy Storage: Solid Solution Modification, Metal/Metallic Oxide Doping, Defect Engineering and Process Optimizing. *Crystals* **2023**, *13*, 295. [CrossRef]
28. Li, H.; Zhou, S.; Zhao, J.; Yan, T.; Du, Y.; Zhou, H.; Pu, Y.; Wang, D. Dielectric temperature stability and energy storage performance of NBT-based lead-free ceramics for Y9P capacitors. *J. Adv. Dielectr.* **2022**, *12*, 2242007. [CrossRef]
29. Tihtih, M.; Ibrahim, J.; Basyooni, M.; Kurovics, E.; Belaid, W.; Hussainova, I.; Kocserha, I. Role of A-site (Sr), B-site (Y), and A, B sites (Sr, Y) substitution in lead-free $BaTiO_3$ ceramic compounds: Structural, optical, microstructure, mechanical, and thermal conductivity properties. *Ceram. Int.* **2023**, *49*, 1947–1959. [CrossRef]
30. Tihtih, M.; Ibrahim, J.; Basyooni, M.; En-nadir, R.; Hussainova, I.; Kocserha, I. Functionality and Activity of Sol-Gel-Prepared Co and Fe co-Doped Lead-Free BTO for Thermo-Optical Applications. *ACS Omega* **2023**, *8*, 5003–5016. [CrossRef]
31. Long, C.; Zhou, W.; Liu, L.; Song, H.; Wu, H.; Zheng, K.; Ren, W.; Ding, X. Achieving excellent energy storage performances and eminent charging-discharging capability in donor (1−x)BT-x(BZN-Nb) relaxor ferroelectric ceramics. *Chem. Eng. J.* **2023**, *459*, 141490. [CrossRef]
32. Tang, W.; Xu, Q.; Liu, H.; Yao, Z.; Hao, H.; Cao, M. High energy density dielectrics in lead-free $Bi_{0.5}Na_{0.5}TiO_3$–$NaNbO_3$–$Ba(Zr_{0.2}Ti_{0.8})O_3$ ternary system with wide operating temperature. *J. Mater. Sci. Mater. Electron.* **2016**, *27*, 6526–6534. [CrossRef]
33. Zhang, L.; Pu, Y.; Chen, M. Ultra-high energy storage performance under low electric fields in $Na_{0.5}Bi_{0.5}TiO_3$-based relaxor ferroelectrics for pulse capacitor applications. *Ceram. Int.* **2020**, *46*, 98–105. [CrossRef]
34. Wu, Y.; Fan, Y.; Liu, N.; Peng, P.; Zhou, M.; Yan, S.; Cao, F.; Dong, X.; Wang, G. Enhanced energy storage properties in sodium bismuth titanate-based ceramics for dielectric capacitor applications. *J. Mater. Chem. C* **2019**, *7*, 6222–6230. [CrossRef]
35. Wang, H.; Yuan, H.; Li, X.; Zeng, F.; Wu, K.; Zheng, Q.; Fan, G.; Lin, D. Enhanced energy density and discharged efficiency of lead-free relaxor $(1-x)[(Bi_{0.5}Na_{0.5})0.94Ba_{0.06}]0.98La_{0.02}TiO_3$-$xKNb_{0.6}Ta_{0.4}O_3$ ceramic capacitors. *Chem. Eng. J.* **2020**, *394*, 124879. [CrossRef]
36. Zhang, L.; Pu, Y.; Chen, M. Influence of $BaZrO_3$ additive on the energy-storage properties of $0.775Na_{0.5}Bi_{0.5}TiO_3$-$0.225BaSnO_3$ relaxor ferroelectrics. *J. Alloy. Compd.* **2019**, *775*, 342–347. [CrossRef]
37. Qiao, X.; Zhang, F.; Wu, D.; Chen, B.; Zhao, X.; Peng, Z.; Ren, X.; Liang, P.; Chao, X.; Yang, Z. Superior comprehensive energy storage properties in $Bi_{0.5}Na_{0.5}TiO_3$-based relaxor ferroelectric ceramics. *Chem. Eng. J.* **2020**, *388*, 124158. [CrossRef]
38. Shi, P.; Zhu, L.; Gao, W.; Yu, Z.; Lou, X.; Wang, X.; Yang, Z.; Yang, S. Large energy storage properties of lead-free $(1-x)(0.72Bi_{0.5}Na_{0.5}TiO_3$-$0.28SrTiO_3)$-$xBiAlO_3$ ceramics at broad temperature range. *J. Alloy. Compd.* **2019**, *784*, 788–793. [CrossRef]
39. Zhang, J.; Lin, Y.; Wang, L.; Yang, Y.; Yang, H.; Yuan, Q. Significantly enhanced energy storage density in sodium bismuth titanate-based ferroelectrics under low electric fields. *J. Eur. Ceram. Soc.* **2020**, *40*, 5458–5465. [CrossRef]
40. Xu, Q.; Liu, H.; Xie, J.; Zhang, L.; Luo, W.; Huang, X.; Cao, M.; Hao, H.; Yao, Z.; Lanagan, M. High-Temperature Dielectrics in BNT-BT-Based Solid Solution. *IEEE Trans. Ultrason. Ferroelectr. Freq. Control* **2016**, *63*, 1656–1662. [CrossRef]
41. Yao, Y.; Li, Y.; Sun, N.; Du, J.; Li, X.; Zhang, L.; Zhang, Q.; Hao, X. Enhanced dielectric and energy-storage properties in ZnO-doped $0.9(0.94Na_{0.5}Bi_{0.5}TiO_3-0.06BaTiO_3)-0.1NaNbO_3$ ceramics. *Ceram. Int.* **2018**, *44*, 5961–5966. [CrossRef]
42. Zhao, X.; Bai, W.; Ding, Y.; Wang, L.; Wu, S.; Zheng, P.; Li, P.; Zhai, J. Tailoring high energy density with superior stability under low electric field in novel $(Bi_{0.5}Na_{0.5})TiO_3$-based relaxor ferroelectric ceramics. *J. Eur. Ceram. Soc.* **2020**, *40*, 4475–4486. [CrossRef]
43. Yang, L.; Kong, X.; Li, F.; Hao, H.; Cheng, Z.; Liu, H.; Li, J.; Zhang, S. Perovskite lead-free dielectrics for energy storage applications. *Prog. Mater Sci.* **2019**, *102*, 72–108.
44. Zhu, Z.; Luo, L.; Wang, F.; Du, P.; Zhou, X.; Zhang, Q.; Li, W.; Wang, Y. Improved Depolarization Temperature via the Ordered Alignment of Defect Dipoles in $(Na_{0.5}Bi_{0.5})TiO_3$-$BaTiO_3$ Ceramics. *J. Eur. Ceram. Soc.* **2020**, *40*, 689–698. [CrossRef]
45. Zhang, X.; Hu, D.; Pan, Z.; Lv, X.; He, Z.; Yang, F.; Li, P.; Liu, J.; Zhai, J. Enhancement of Recoverable Energy Density and Efficiency of Lead-free Relaxor-ferroelectric BNT-based Ceramics. *Chem. Eng. J.* **2021**, *406*, 126818. [CrossRef]
46. Liu, Z.; Dong, X.; Liu, Y.; Cao, F.; Wang, G. Electric field tunable thermal stability of energy storage properties of PLZST antiferroelectric ceramics. *J. Am. Ceram. Soc.* **2017**, *100*, 2382–2386. [CrossRef]